Gayathri, K., Radhika, R., Shankar, R., Malathi, M., Savithiri, K., Sparkes, H. A., ... Mohan, P. S. (2017). Comparative theoretical and experimental study on novel tri-quinoline system and its anticancer studies. *Journal of Molecular Structure*, *1134*, 770-780. https://doi.org/10.1016/j.molstruc.2017.01.030

Comparative theoretical and experimental study on novel tri-quinoline system and its anticancer studies

Kasirajan Gayathri [a], Ramachandran Radhika [b], Ramasamy Shankar [b], Mahalingam Malathi [c], Krishnaswamy Savithiri [a], Hazel A. Sparkes [d], Judith A.K. Howard [e], Palathurai Subramaniam Mohan [a*]

[a] *Department of Chemistry, Bharathiar University, Coimbatore 641 046, Tamil Nadu, India*
[b] *Department of Physics, Bharathiar University, Coimbatore 641 046, Tamil Nadu, India*
[c] *Department of Chemistry, Bannari Amman Institute of Technology, Sathyamangalam 638 401, Tamil Nadu, India*
[d] *School of Chemistry, University of Bristol, Cantock's Close, Bristol, BS8 1TS, UK*
e Department of Chemistry, Durham University, South Road, Durham, DH1 3LE, UK

E-mail address: ps_mohan_in@yahoo.com, psmohan59@gmail.com (P.S. Mohan).
**Corresponding author. Tel.: +919363211210*

Abstract

A novel compound 2-chloro-3,6-bis-(quinolin-8-yloxymethyl)-quinoline **3** bearing a tri-quinoline moiety has been synthesized from 2-chloro-3,6-dimethyl quinoline **1** and 8-hydroxy quinoline **2** using dry acetone and K_2CO_3 as a base. **3** has been characterized by using FT-IR, FT-Raman, UV-Vis, ^{1}H NMR, ^{13}C NMR spectra and single crystal X-ray diffraction methods. We have also made a combined experimental and theoretical study on the molecular structure, vibrational spectra, NMR, FT-IR, FT-Raman and UV-Vis spectra of 2-chloro-3,6-bis-(quinolin-8-yloxymethyl)-quinoline. The theoretical studies of the title compound have been evaluated by using density functional theory calculations using B3LYP/6-31+G(d,p) and M06-2X/6-31+G(d,p) level of theories. The calculated theoretical values were found to be in good agreement with the experimental findings. The single crystal structure **3** crystallized in the orthorhombic space group *Pna*2_1. The compound **3** exhibits higher cytotoxicity in human cervical cancer cell lines (HeLa) than human breast cancer cell lines (MCF7).

Highlights

- A novel tri-quinoline was synthesized and optimized by density functional theories.
- Single crystal XRD, FT-IR, Raman, ^{1}H, ^{13}C NMR and UV-Vis spectra were studied.
- All the experimental data were compared with theoretical values.
- Cytotoxicity was determined by MTT assay and by theoretical calculations.

Keywords

2-chloro-3,6-bis-(quinolin-8-yloxymethyl)-quinoline

Spectroscopic studies

Single crystal XRD

MEP

HOMO-LUMO

Cytotoxicity

Introduction

The compounds of quinoline based derivatives find extensive applications such as medicinal usage, material utility, optoelectronic properties etc. Specifically, 8-hydroxy quinoline (8HQ) is used as one of the components in organic light emitting diode (OLED) fabrication [1, 2] since the organic materials have photoconductive, photorefractive and hole transporting properties[3]. 8HQ is extensively used as the best chelator[4-7] for metal ions after Ethylenediaminetetraacetic acid (EDTA) due to its chromogenic behavior. Derivatives of 8-hydroxy quinoline have been popular in the field of organometallic chemistry[8, 9] and as a fluorescent sensors[10, 11] because of the ease of complex formation with various metal ions such as Ag^{+}[12], Cd^{2+}[10], Cu^{2+}[13, 14]. Also the special properties of quinolates were

illustrated by simple Werner -type complexes and have been useful in the synthesis of metallosupramolecular materials [15, 16]. 8HQ derivatives and their quinolates are known to possess therapeutic properties for Alzheimer's disease[17], widely used as antimicrobial[18, 19] and antitumor agents[20, 21] To prepare newer derivatives, an elaborate knowledge of spectroscopic and stability behavior is required in order to promote the utility value in medicinal properties.

In recent years, density functional theory (DFT)[22] has been extensively used for optimized structural studies. In the present work, Becke's three parameter hybrid functional[23, 24] with correlation functional of Lee-Yang-Parra[25] (B3LYP) and the hybrid meta-GGA functional M06-2X with 6-31+G(d,p) basis set have been used for comparing the experimental values of geometry, vibrational spectra, electronic and NMR spectra etc.

In this communication, we report the first ever synthesis of the novel tri-quinoline based compound **3** which was synthesized from 2-chloro-3, 6-dimethyl quinoline and 8-hydroxy quinoline using dry acetone and anhydrous K_2CO_3 as a base. Subsequently, we aimed to compare the structural and spectroscopic properties of compound **3** obtained experimentally with theoretical results from density functional theory calculations using B3LYP and M06-2X level of theories. We optimized the structure of compound **3** and the calculations were performed to calculate ^{1}H NMR, ^{13}C NMR, FT-IR, FT-Raman and UV-Vis spectra at the B3LYP and M06-2X level of theories. Furthermore, the frontier molecular orbital energies of compound **3** have been calculated and various molecular properties such as chemical hardness, softness, electrophilicity, electronegativity, ionization potential, chemical potential and electron affinity have also been observed at these theory levels. From the molecular electrostatic potential (MEP), the lowest unoccupied molecular orbital (LUMO) and highest occupied molecular orbital (HOMO) were plotted to visualize the charge distributions and electronic transport properties of compound **3**. The comparisons between experimental and theoretical calculations have also been done.

Materials and methods

Experimental

General

All reagents and chemicals were of analytical grade and purchased from Sigma Aldrich. The solvents were purified by standard methods. Thin layer chromatography (TLC) plates coated with silica gel containing 13% calcium sulfate as a binder were used to test the purity of the compound. Melting point (M.P., ºC) was determined using Mettler FP 51 apparatus (Mettler Instruments, Switzerland) and remains uncorrected. Microanalyses were performed on a Vario EL III model CHNS analyzer (Vario, Germany).

*FT-IR, FT-Raman, UV spectra and NMR analysis of compound **3***

The IR spectrum of compound **3** was recorded using KBr pellets in the scan range of 4000-400 cm^{-1} with a resolution of 4 cm^{-1} on a Nicolet Avatar Model FTIR spectrometer (with ESP DTGS detector). Raman spectrum was measured using JY-1058 Raman spectrometer (with CCD detector) in the scan range of 4000-50 cm^{-1} with resolution of 2 cm^{-1}. ^{1}H NMR and ^{13}C NMR were recorded using a Bruker 400 MHZ and 100 MHz spectrometers respectively using tetramethyl silane (TMS) as an internal standard reference and dimethyl sulfoxide-d_6 as solvent. The chemical shift values were recorded as δ (ppm). UV–Visible absorption spectrum of compound **3** (1×10^{-3} M solution in EtOH/H_2O 1:1(v/v)) was recorded at 24 ± 1º C using JASCO-V- 630 spectrophotometer.

Single crystal X-ray analysis

X-ray diffraction data for **3** were collected at 100(2) K on a Bruker APEX II CCD diffractometer using Mo-K_α radiation (λ = 0.71073 Å). Absorption corrections were based on equivalent reflections using SADABS[26]. The structure was solved using SHELXS[27] and refined against F^2 in SHELXL[28] using Olex2[29]. All of the non-hydrogen atoms were

refined anisotropically, while all of the hydrogen atoms were located geometrically and refined using a riding model. There was disordered solvent present in the lattice which could not be sensibly modelled so Squeeze within Platon [30] was used to treat this. Crystal structure and refinement data are given in Table 1. The structure has the CCDC number 1005001. Copies of the data can be collected, free of charge, on application to CCDC, 12 Union Road, Cambridge, CB2 1EZ, UK. [Fax: + 44(0)-1223-336033 or e-mail: deposit@ccdc.cam.ac.uk].

DFT computational analysis

The molecular geometry for the compound **3** has been extracted from the single crystal X-ray analysis data. The compound **3** was optimized by using B3LYP and M06-2X level of theories with 6-31+G(d,p) basis set in the Gaussian 09 suite of program[31]. The vibrational frequencies were found at these theory levels and no imaginary frequencies were observed which confirmed that the structure is on the real minima. Due to the absence of anharmonicity in the system, calculated stretching frequencies were higher than experimental values. The values were scaled by 0.964[32] and 0.979[33] at the B3LYP and M06-2X level of theories respectively and agreed well with the experimental values. The UV-Vis spectra were calculated using polarizable continuum model (PCM)[34] in ethanol solution by using the time-dependent density functional theory (TD-DFT). The NMR chemical shift calculations were done by using the Gauge-Independent Atomic Orbital (GIAO) method[35] at B3LYP and M06-2X level of theories with 6-31+G(d,p) basis set. The molecular electrostatic potential map is plotted for the optimized structure of the title compound **3** and it shows the probable electrophilic and nucleophilic sites of the molecule.

Cytotoxicity study by MTT (3-(4,5-dimethylthiazol-2-yl)-2,5-diphenyltetrazolium bromide) assay

A cytotoxicity study of compound **3** was carried out on human liver cancer cells (A549) which were collected from National Centre for Cell Science (NCCS), Pune, India. Cell viability was carried out using the MTT assay method. Cells were maintained in Eagles minimum essential medium containing 10% fetal bovine serum (FBS). For the screening experiment, the

cells were seeded into 96-well plates in 100 µL of the respective medium containing 10% FBS, plates with a density of 10000 cells/well and incubated in a humidified incubator at 37 °C, using conditions of 5% CO_2, 95% air and 100% relative humidity for 24 h prior to the addition of compound. The compound **3** was dissolved in DMSO and diluted in the respective medium containing 1% FBS. After 24 h, the medium was changed with the respective medium with 1% FBS containing the compounds at various concentrations and incubated at 37 °C with conditions of 5% CO_2, 95% air and 100% relative humidity for 48 h. Triplication was maintained and the medium not containing the compound served as the control. After 48 h, 10 µL of MTT (5 mg/mL) in phosphate buffered saline (PBS) was added to each well and incubated at 37 °C for 4 h. The medium with MTT was then flicked off and as a result formazan crystals were dissolved in 100 µL of DMSO. The absorbance was then measured at 570 nm using a microquant plate reader (Bio-Tek Instruments). The percentage of cell inhibition was determined using the formula

% of inhibition = [mean OD of untreated cells (control) / mean OD of treated cells] × 100

and a graph was plotted as the percentage of cell inhibition versus concentration and from this the IC_{50} value was calculated.

Results and discussion

Chemistry

8-hydroxy quinoline (0.025 g, 0.26 mmol) was added to the solution of 3,6-bis(bromomethyl)-2-chloroquinoline[36] (0.048 g, 0.13 mmol) in dry acetone along with anhydrous K_2CO_3 (10 mg). The reaction mixture was refluxed at 100-120 ºC for 8 h. After completion of the reaction, the mixture was cooled to room temperature and using reduced pressure the excess solvent was removed to get a yellow oil that was separated by silica gel column chromatography (80:20 *v/v* Petroleum ether: Ethyl Acetate) to give pure compound **3** in 64 % yield; Mp: 223 °C; IR (KBr, cm^{-1}) 3041, 1699, 1559, 1378, 1008, and 702; ^{1}H NMR (300 MHz, DMSO, ppm): δ 8.84-8.85 (m, 2H, Ar-H), 8.33(m, 2H, Ar-H), 8.29 (d, 2H, *J*= 8.4 Hz, Ar-H), 8.05(s, 1H, Ar-H), 7.94(d, 2H, *J*= 8.8 Hz, Ar-H), 7.87(d, 2H, *J*= 8.8 Hz, Ar-H), 7.45-7.53(m,

4H, Ar-H), 7.29(d, 1H, *J*= 7.2 Hz, Ar-H), 5.48(s, 4H, CH_2); ^{13}C NMR (100 MHz, DMSO, ppm): 154.07, 153.70, 149.64, 149.51, 146.84, 136.80, 136.22, 136.10, 136.01, 129.72, 129.63, 129.43, 129.03, 128.75, 127.29, 126.65, 126.53, 125.78, 121.88, 121.74, 120.83, 120.36, 110.12, 110.10, 70.33, 67.37; $C_{29}H_{20}N_3O_2Cl$: Calculated C 72.88 %; H 4.22 %; N 8.79 %; Found, C 72.84 %; H 4.49 %; N 8.28 %.

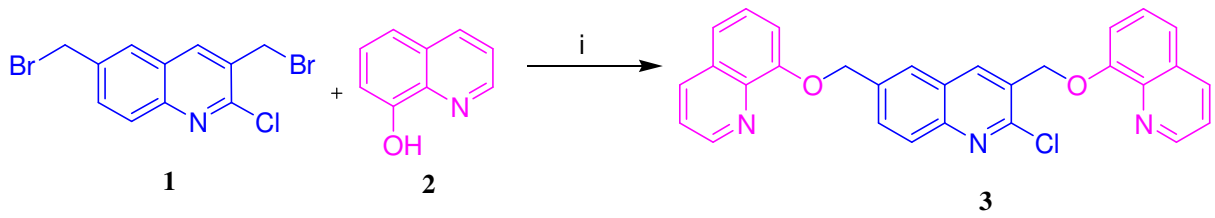

1 **2** **3**

i) Dry Acetone, Anhydrous K_2CO_3, Reflux, 100 ℃

Scheme 1: Synthesis of 2-Chloro-3,6-bis-(quinolin-8-yloxymethyl)-quinoline **3**

Single crystal X-ray diffraction studies

The structure of **3** was confirmed by single crystal X-ray diffraction, see Fig. 1. It crystallized in the orthorhombic space group *Pna*2_1 with one molecule in the asymmetric unit. One of the terminal quinolines (N2, C11-C19) was in almost the same plane as the central Cl substituted quinoline (N1, C1-C9) with a plane to plane angle of ~2° while the second terminal quinoline (N3, C21-C29) was twisted significantly, ~62°, out of the place of the rest of the molecule. The structure contained π-π stacking interactions between the central quinolone (N1, C1-C9) and terminal quinolone (N2, C11-C19), with centroid-centroid distances of ~3.6 Å and a shift of ~1.4 Å. Disordered solvent was removed through the use of Squeeze.

FT NMR analysis

^1H NMR and ^{13}C NMR spectra were observed in DMSO-d_6 using TMS as an internal standard. ^1H NMR and ^{13}C NMR data of compound **3** are tabulated in Table 3. In ^1H NMR, four protons of two CH_2 groups appeared in the upfield region of δ 5.48 ppm. All other aromatic

proton peaks were observed in the downfield region between δ 7.45 and 8.85 ppm. ^{13}C NMR spectrum showed the presence of 26 carbon atoms. The characteristic signals at δ 67.37 and δ 70.33 ppm were due to -CH_2 group carbon atoms. The aromatic carbons appeared in the region between δ 110.10 and δ 154.07 ppm (Fig. S2).

In vitro cytotoxicity assay

By using MTT assay, the *in vitro* cytotoxicity of the compound **3** was done against human cervical cancer cell lines (Hela) and human breast cancer cell lines (MCF7).

XRD studies and structural analysis

The bond lengths, bond angles and dihedral angles of compound **3** from the single crystal XRD data are tabulated in accordance with the atom numbering scheme as shown in Fig. 1. The experimental and theoretical results of bond lengths, bond angles and dihedral angles are compared and tabulated in Tables S1, S2 and S3. The optimized bond lengths and bond angles are calculated and are slightly varied from the experimental values because the structure of compound **3** is optimized in gas phase while in X-ray diffraction the molecule is packed in a crystal in addition the crystal structure contained disordered solvent that was squeezed out but may alter the molecular geometry, although this does not appear to have been very significant here.

Both the experimental and theoretical X-ray data show single and double bonds for C-C in the quinoline heterocyclic compounds. The experimental X-ray structure showed C-C bond length in the range of aromatic 1.346(6)-1.436(5) Å, single 1.498(5)-1.506(5) Å and their corresponding theoretical C-C bond lengths are formed around aromatic 1.375-1.439 Å, single 1.51-1.509 Å using B3LYP and M06-2X level of theories. The experimental C-Cl and C-N bond lengths in compound **3** are 1.776(3) Å and 1.300(4)-1.376(4) Å respectively with the related theoretical bond lengths 1.775 Å and 1.28-1.367 Å respectively. Hence a good agreement is found between the bond lengths of experimental and theoretical results.

In quinoline ring, almost all the bond angles of carbon lie around 120º, with sp^2 hybridization for their corresponding carbon atoms. The ∠CCC was found in the range of 116.5(3)-123.9(4)º and 116.1-123.2º for experimental and theoretical data respectively. The experimental bond angles of C11-O1-C10 and C21-O2-C20 were found as 115.8(3) Å and 116.9(3) Å respectively while the theoretical values were calculated as 116.2 Å and 118.7(B3LYP) and 119.5 Å and 119.5 Å(M06-2X). The bond lengths of C-N, C=N, C-Cl, C-O, C-H, C-C agree well with the correlation coefficient of 0.9742 while the correlation coefficients of bond angles of C-C-C, C-C-N, C-N-C, C-C-Cl, O-C-H, C-O-C is 0.9612. The correlation coefficient of experimental and theoretical dihedral angles of O-C-C-C, N-C-C-C, and N-C-C-O is 0.9988 (Fig. S1). From the obtained results almost all the experimental bond lengths, bond angles and dihedral angles quite agreeable with theoretical observations.

Quantum Theory of Atoms In Molecules (QTAIM)[37] is an important tool to describe the chemical bonding between the atoms. To observe the orientation of the molecule, QTAIM calculation were done to investigate the contributions of the intramolecular hydrogen bonds and Van der Waals interactions by using MORPHY 98 program package[38]. Surprisingly, no such interactions were observed in compound **3**. Thus for the orientation of the compound **3**, the impact of non-covalent interaction is lacking.

FT-IR and FT-Raman assignments

The infrared and Raman spectra of compound 2-chloro-3,6-bis-(quinolin-8-yloxymethyl)-quinoline **3** are carried out in the frequency range of 4000-400 cm^{-1} and 4000-50 cm^{-1} respectively. The FT-IR and FT-Raman spectra of the molecule have been calculated by using B3LYP and M06-2X level of theories with 6-31+G(d,p) basis set. The calculated vibrational frequencies of FT-IR and FT-Raman, their IR intensities, Raman activities and their corresponding experimental frequencies were compared in Table 2. The experimental and theoretical FT-IR and FT-Raman were shown in the Figs. 2 and 3.

C-C vibrations

The FT-IR and FT-Raman stretching frequencies for the aromatic ring and C-C were calculated by using B3LYP/6-31+G(d,p) and M06-2X/6-31+G(d,p) level of theories. The carbon-carbon stretching vibrations in phenyl ring are identified with reference to the previously reported vibrations of the benzene molecule[39, 40]. The C-C stretching vibrations are very important modes in carbon skeleton molecule. From the literature studies[41], the C-C stretching vibrations are observed in the region 1625-1430 cm^{-1}. In our present study, the experimental C-C stretching vibrations were observed between 1428-1378 cm^{-1} for FT-IR and 1422 cm^{-1} for FT-Raman. For the titled compound, the corresponding theoretical FT-IR and FT-Raman stretching vibrations were observed at 1379-1355 cm^{-1} and 1403-1381 cm^{-1} using B3LYP and M06-2X level of theories respectively which agree well with the experimental FT-IR and FT-Raman values.

C-H and C=N vibrations

In most of the aromatic compounds, C-H stretching vibrations[42] are usually observed at 3100-2850 cm^{-1} and in the present investigation, they were observed at 3165-3005 cm^{-1} in FT-IR and FT-Raman spectra by B3LYP/6-31+G(d,p) and M06-2X/6-31+G(d,p) methods. Experimentally, the bands observed at 3188 and 3041 cm^{-1} were attributed to C-H stretching modes. According to Silverstein *et al*[43], the C=N ring stretching bands are observed in the region of 1600-1430 cm^{-1}. The experimentally calculated C=N stretching vibrations were observed at 1699 and 1568 cm^{-1} for FT-IR and FT-Raman values respectively and theoretical values of FT-IR and FT-Raman spectra were calculated around 1602, 1601 and 1590 cm^{-1} at B3LYP level of theory which has been associated to C=N stretching vibrations of compound **3**. While, by using M06-2X functional the values were calculated at 1633, 1641 and 1656 cm^{-1}.

C-Cl and C-O vibrations

In quinoline ring, C-Cl stretching is observed as a very intense and narrow peak in the range of 850-550 cm^{-1} [44]. Arjunan *et al*[45] reported C-Cl stretching vibration at 734 cm^{-1} for

IR and 735 cm^{-1} for Raman. In our current investigation, C-Cl stretching vibrations of the compound **3** have been observed at 702 cm^{-1} and 768 cm^{-1} for FT-IR and FT-Raman respectively and the corresponding theoretical values have been calculated at 746 and 773 cm^{-1} for FT-IR and FT-Raman at B3LYP and M06-2X level of theories respectively. According to the literature[46], the stretching mode of C-O is observed around 1350-1000 cm^{-1}. The bands observed around at 1317, 1316, 1332 and 1330 cm^{-1} in FT- IR and FT-Raman have been assigned to C-O stretching vibrations of the compound which have been calculated at the B3LYP and M06-2X level of theories. The experimental values of C-O stretching vibrations are observed at 1378 cm^{-1} and 1385 cm^{-1} in FT-IR and FT-Raman values respectively.

CH_2 vibrations

Basically there are six fundamentals stretching modes linked with each CH_2 group. They are CH_2 asym-asymmetric stretching, CH_2 sym- symmetric stretching, CH_2 scis-scissoring and CH_2 rock-rocking modes and are expected to be polarized. The CH_2 wag-wagging and CH_2 twist-twisting modes belong to depolarized for out of plane bending vibrations[47]. In the present investigation, the experimental CH_2 symmetric and asymmetric FT-IR vibrational frequencies were found at 3041 cm^{-1} respectively and the corresponding CH_2 symmetric and asymmetric stretching frequencies of FT-Raman are noted at 3064 cm^{-1}. The theoretical values of the FT-IR and FT-Raman associated to symmetric CH_2 stretching vibrational frequencies of title compound have been calculated at 2851, 2869 and 2969, 2986 cm^{-1} at B3LYP/6-31+G(d,p) and M06-2X/6-31+G(d,p) level of theories. While the asymmetric CH_2 stretching vibrational frequencies were noticed at 2898 and 2903 cm^{-1} for B3LYP and 3018 and 3031 cm^{-1} for M06-2X level of theories. Both theoretical and experimental CH_2 symmetric as well as asymmetric stretching vibrational frequencies are in good agreement with each other. Similarly all the possible modes of vibrations are tabulated in Table 2 by using B3LYP and M06-2X level of theories with 6-31+(d,p) as basis set. In addition, the CH_2 bending and stretching modes follow the order of decreasing wave number and the order is CH_2 scissoring> CH_2 >wagging >CH_2 twisting > CH_2 rocking[48, 49]. All the CH_2 vibrations were computed at the B3LYP and M06-2X level of theories which agreed well with the experimental values.

NMR analysis

^{1}H and ^{13}C NMR spectra of the title compound were recorded by using DMSO-d_6 solvent and TMS as the internal standard and the chemical shift values were (δ) calculated by B3LYP/6-31+G(d,p) and M06-2X/6-31+G(d,p) (Fig. S2). The experimental ^{1}H and ^{13}C chemical shift values are compared with the theoretically calculated ^{1}H and ^{13}C chemical shift values and are presented in Table 3. The theoretically calculated chemical shift values of aliphatic protons were observed in the shielded region of 4.83-5.11 ppm and experimentally a sharp singlet is observed at 5.48 ppm which is attributed to two CH_2 protons. The experimental chemical shifts were obtained in the deshielded region of 7.29-8.84 ppm which is attributed to aromatic ring protons while the theoretical values are found in the region of 6.57-9.01 and 7.55-10.36 ppm by using B3LYP and M06-2X level of theories respectively.

In ^{13}C NMR, the experimental chemical shift values of the aromatic carbons have appeared in the region of 120.36-149.64 ppm. In the present investigation, theoretically calculated chemical shift values of ^{13}C aromatic carbons were found to be in the range of 105.88 to 143.37 ppm. In addition to that, aliphatic carbons C21 and C41 (carbon atoms are numbered using fig. 1b) give a signal in the upfield region at 67.37 and 70.33 ppm respectively with the corresponding theoretical values of 57.89 and 61.82 ppm (B3LYP) and 53.82 and 59.44 ppm (M06-2X). As the compound **3** contains a Cl group which is an electronegative functional group, it polarizes the electron distribution. In ^{13}C NMR, the experimental chemical shift value of C47 bonded to Cl group is too high as observed in the downfield region of 154.07 ppm and the corresponding theoretical ^{13}C NMR chemical shift of Cl group is noted at 141.28 ppm. From the Table 3, the difference between experimental and theoretical values is in the range of 0.004 to 2.31 ppm and 0.3 to 32 ppm for the ^{1}H and ^{13}C NMR respectively. Theoretical data of ^{1}H and ^{13}C chemical shift values are in good agreement with the experimental data since, the error between the theoretical and experimental values can up to 30 ppm[50]. The experimental and theoretical NMR chemical shift values are portrayed by using Root Mean Square Deviation by Linear regression plot given in Figure S3. From the figure it is found that the correlation coefficient obtained for the ^{1}H and ^{13}C NMR at B3LYP and M06-2X level of theories are found as 0.9538,

0.9661, 0.8751 and 0.8750 respectively which represent the good correlation between the experimental and theoretical values.

Molecular electrostatic potential

The electrostatic potential map (MEP) is used to visualize the charge distributions in molecules, the size and shape of molecules along with the charge-related properties of molecules[51, 52]. The molecular electrostatic potential V(r) is defined as

$$V(r) = \sum_{A} \frac{Z_A}{(R_A - r)} - \int \frac{\rho(r')}{(r' - r)}\, d(r')$$

where Z_A is the charge of nucleus A, located at R_A, ρ(r') is the electronic density function of the compound. A molecular electrostatic potential map (MEP) was used to visualize the charge distributions over compound **3** and identify the reactive sites of the compound.

Using the density functional B3LYP with 6-31+G(d,p) basis set, the MEP was plotted over the optimized geometry of molecule **3**. In MEP, the red color refers to negative electrostatic potential regions (electron-rich) which are related to electrophilic attack while blue color refers to positive electrostatic potential regions (electron-poor) which are related to nucleophilic attack. The green color refers to zero electrostatic potential. From Fig. 4, it is observed that compound **3** has several possible sites for electrophilic attack. These negative sites in compound **3** were found around the N1, N2 and N3 atoms as -0.102, -0.190 and -0.178 a.u respectively in the quinoline ring and negative potential is also found around O1 and O2 atoms of ether linkage as -0.345 and -0.300 a.u. From the obtained values, it is clear that a greater electrophilic region is found around the oxygen atoms O1 and O2 of the ether linkage. This might be due to the presence of delocalization of charge around the oxygen atoms. The positive potential regions are highly localized over the hydrogen atoms of the quinoline rings which are susceptible to nucleophilic attack and the corresponding positive charges are in the range of 0.176- 0.248 a.u. In general, halogen atoms are electronegative which favors electrophilic attack. However, in the present work, green color in the MEP indicates the radical attacking site due to the Cl atom and the corresponding charge value is 0.088 a.u.

Frontier molecular orbitals (HOMO and LUMO)

The HOMO energy represents the electron donating ability while the LUMO represents the electron-accepting ability of the molecule. The Eigen values of HOMO and LUMO designate the chemical stability and reactivity of a molecule[53]. The frontier molecular orbitals play an important role in describing the HOMO, LUMO energies and were calculated by using B3LYP/6-31+G (d,p) and M06-2X/6-31+G (d,p).

The frontier molecular orbital[54] is very useful in determining the electrical transport properties of the molecules. HOMO and LUMO values are used in determining the chemical reactivity, kinetic stability, chemical hardness and softness of the compound, properties that are used to describe the bioactivity of a molecule *via* intermolecular charge transfer[55]. A molecule with a large HOMO-LUMO energy gap is more stable, less polarizable and with less chemical reactivity is said to be hard species while a molecule with a small HOMO-LUMO gap is said to be soft species[56].

According to Koopmans theorem[57], from the HOMO and LUMO energy values, ionization potential (I), chemical potential(μ), electron affinity (A), chemical hardness (η) and electrophilicity (ω) were calculated and the results are shown in Table 4. The calculated HOMO and LUMO values of the compound **3** are -6.0836 and -1.7957 eV (B3LYP) and -7.3574 and 0.9377 eV (M06-2X). The HOMO-LUMO energy gap of the compound **3** is 4.28800 eV and -6.4197 eV at B3LYP and M06-2X level of theories. The energy distributions and levels of HOMO-3, HOMO-2, HOMO-1, HOMO, LUMO+1, LUMO+2, LUMO+3 orbitals computed by using B3LYP/6-31+G(d,p) level of theory are shown in Figs. 5 and S4. The HOMO of the compound **3** is localized over the 6-substituted quinoline and LUMO is distributed over the Cl-substituted and 3-substituted quinoline.

Electrophilicity (ω) is used to determine the energy lowering due to electron flow between an acceptor and donor[58]. Recently, Bondarchuk *et al* [59, 60] reported the modern developments of electrophilicity concepts. To calculate the global (ω) and local electrophilicity (ω_k^+) indexes, vertical and adiabatic approaches have been used and the experimental data

supports the adiabatic approach. This index is also useful in finding out the toxicity value in terms of site selectivity and reactivity[61]. In our present work, the toxicity values (log $1/IC_{50}$) can be determined by the regression equation given below

$$\log[1/IC_{50}] = 3.3944*\omega - 5.5788.$$

The above equation was tested for aliphatic amines, polychlorinated dibenzofurans and polychlorinated biphenyls against ciliate fresh water protozoa *Tetrahymena pyriformis* [62] where electrophilicity index (ω) is taken as an independent variable. Cell viability graphs of compound **3** using MTT assay are shown in Fig. S5. The IC_{50} value by MTT assay was calculated as 21.02 µM and 27.73 µM against HeLa and MCF-7 cancer cell lines. The toxicity values (log $1/IC_{50}$) were observed as 19.61 µM and 10.48 µM at B3LYP and M06-2X level of theories respectively which are comparable with the experimental values.

Electronic spectra

The electronic absorption spectrum of the title compound **3** was recorded in the range 200-600 nm using the solvent as ethanol and the representative spectrum is given in Fig. 6. From the figure, it can be observed that the electronic absorption spectrum showed one maximum at 233 nm are caused by the n-π* transitions and two strong shoulder bands at 315 and 364 nm might be due to π-π*. This spectral absorption is similar to those found in related quinoline compounds [63, 64].

The TD-DFT/ B3LYP/6-31+G(d,p) calculations were done for the optimized structure of the compound **3** in ethanol solvent using PCM model. The stimulated UV-Vis spectra are shown in Fig. 6. From the calculations, it is observed that by using the B3LYP level of theory, the computed absorption wavelengths are obtained at 286.08, 291.31, 317.14, 319.96, 331.75 nm. For M06-2X, the theoretical absorption values were found to be 241.62, 258.81, 268.60, 281.42, 349.77 nm. The calculated values along with their oscillator strength (f) and the experimental values are listed in Table 5. Thus theoretical absorption values are in good agreement with the experimental value.

Conclusion

The present work reports a novel tri-quinoline compound which has been synthesized to find out the anticancer activity. In order to resolve the unambiguity of the structure both by theoretical and experimental studies, complete spectroscopic studies FT-IR, FT-Raman, ^{1}H NMR, ^{13}C NMR, UV- Vis, HOMO and LUMO were undertaken and found to be in agreement with the experimental values of the synthesized compound. By using the PCM model, the absorption maximum (λ_{max}) of the compound was found by TD-DFT calculations and compared with the experimental spectra. Most of the experimental data were found to be in good agreement with the theoretical results. It has been noticed that the experimental data were obtained in solid phase while all the theoretical calculations were done in gaseous phase except the electronic spectrum which was calculated in solvent phase. The small difference in the results might be due to the phase used. The study also revealed some interesting facts in terms of studying the possible electrophilic and nucleophilic sites of the compound using molecular electrostatic potential map and showed that the positive potential regions are around the hydrogen atoms while the negative potential regions are on electronegative atoms. The eventual charge transfer interactions were studied using frontier orbital analysis. IC_{50} of the compound was found to be 21.02 µM and 27.73 µM against HeLa and MCF-7 cancer cell lines using MTT assay and is in agreement with the theoretical data.

Acknowledgement

Our sincere thanks go to the SIF, VIT-University, Vellore, for providing access their NMR spectral facilities. P.S.M thanks, DRDO-BU-CLS (DLS/86/50071/DRDO-BU center /Phase-II) for funding. Two of the authors R. S and R. R are thankful to DST-SERB-Fast Track Project grant No: SR/FTP/PS-151/2011 & 22.05.2012 for financial assistance. One of the authors K.S is thankful to the University Grant Commission (UGC-SAP), New Delhi, for BSR - Senior Research Fellowship, which is gratefully acknowledged.

Appendix A. Supplementary material

CCDC 1005001 contains the supplementary crystallographic data for this paper. These data can be obtained free of charge from The Cambridge Crystallographic Data Centre *via* www.ccdc.cam.ac.uk/data_request/cif.

References

[1] F. Papadimitrakopoulos, X.M. Zhang, D.L. Thomsen, K.A. Higginson, A Chemical Failure Mechanism for Aluminum(III) 8-Hydroxyquinoline Light-Emitting Devices, Chemistry of Materials 8(7) (1996) 1363-1365.

[2] C.C. Wu, J.K.M. Chun, P.E. Burrows, J.C. Sturm, M.E. Thompson, S.R. Forrest, R.A. Register, Poly(p-phenylene vinylene)/tris(8-hydroxy) quinoline aluminum heterostructure light emitting diode, Applied Physics Letters 66(6) (1995) 653-655.

[3] H.H. Fong, S.K. So, Hole transporting properties of tris(8-hydroxyquinoline) aluminum (Alq3), Journal of Applied Physics 100(9) (2006) 094502.

[4] V. Prachayasittikul, S. Prachayasittikul, S. Ruchirawat, V. Prachayasittikul, 8-Hydroxyquinolines: a review of their metal chelating properties and medicinal applications, Drug Design, Development and Therapy 7 (2013) 1157-1178.

[5] D.K. Johnson, S.J. Kline, 8-hydroxyquinoline chelating agents, Google Patents, 1991.

[6] A.V. Bordunov, J.S. Bradshaw, X.X. Zhang, N.K. Dalley, X. Kou, R.M. Izatt, Synthesis and Properties of 5-Chloro-8-hydroxyquinoline-Substituted Azacrown Ethers: A New Family of Highly Metal Ion-Selective Lariat Ethers, Inorganic Chemistry 35(25) (1996) 7229-7240.

[7] K.F. Sugawara, H.H. Weetall, G.D. Schucker, Preparation, properties, and applications of 8-hydroxyquinoline immobilized chelate, Analytical Chemistry 46(4) (1974) 489-492.

[8] S.M.S. Haggag, A.A.M. Farag, M. Abdelrafea, Spectral, thermal and optical–electrical properties of the layer-by-layer deposited thin film of nano Zn(II)-8-hydroxy-5-nitrosoquinolate complex, Spectrochimica Acta Part A: Molecular and Biomolecular Spectroscopy 110 (2013) 14-19.

[9] X. Ouyang, G. Wang, H. Zeng, W. Zhang, J. Li, Design and synthesis of 2-substituted-8-hydroxyquinline zinc complexes with hole-transporting ability for highly effective yellow-light emitters, Journal of Organometallic Chemistry 694(21) (2009) 3511-3517.

[10] Z. Li, P. Xi, L. Huang, G. Xie, Y. Shi, H. Liu, M. Xu, F. Chen, Z. Zeng, A highly selective fluorescent chemosensor for Cd(II) based on 8-hydroxyquinoline platform, Inorganic Chemistry Communications 14(8) (2011) 1241-1244.

[11] H. Zhu, J. Fan, J. Lu, M. Hu, J. Cao, J. Wang, H. Li, X. Liu, X. Peng, Optical Cu^{2+} probe bearing an 8-hydroxyquinoline subunit: High sensitivity and large fluorescence enhancement, Talanta 93 (2012) 55-61.

[12] P. Singh, S. Kumar, A unique 'ON–OFF–ON' switch with two perturbations at two different concentrations of Ag^{+}, Tetrahedron Letters 47(1) (2006) 109-112.
[13] P. Singh, R. Kumar, S. Kumar, 9, 10-Bis(8-Quinolinoxymethyl)Anthracene—A Fluorescent Sensor for Nanomolar Detection of Cu^{2+} with Unusual Acid Stability of Cu^{2+}-Complex, Journal of Fluorescence 24(2) (2014) 417-424.
[14] T. Moriuchi-Kawakami, J. Sato, Y. Shibutani, Analytical Sciences 25(3) (2009) 449-452.
[15] M. Albrecht, O. Blau, E. Wegelius, K. Rissanen, A versatile di(8-hydroxyquinoline) building block for supramolecular as well as metallo-supramolecular chemistry, New Journal of Chemistry 23(7) (1999) 667-668.
[16] M. Albrecht, M. Fiege, O. Osetska, 8-Hydroxyquinolines in metallosupramolecular chemistry, Coordination Chemistry Reviews 252(8–9) (2008) 812-824.
[17] K.J. Barnham, E.C.L. Gautier, G.B. Kok, G. Krippner, 8-hydroxy quinoline derivatives, Google Patents, 2004.
[18] A. Yu Shen, C. Pien Chen, S. Roffler, A chelating agent possessing cytotoxicity and antimicrobial activity: 7-Morpholinomethyl-8-hydroxyquinoline, Life Sciences 64(9) (1999) 813-825.
[19] R. Cherdtrakulkiat, S. Boonpangrak, N. Sinthupoom, S. Prachayasittikul, S. Ruchirawat, V. Prachayasittikul, Derivatives (halogen, nitro and amino) of 8-hydroxyquinoline with highly potent antimicrobial and antioxidant activities, Biochemistry and Biophysics Reports 6 (2016) 135-141.
[20] S.H. Chan, C.H. Chui, S.W. Chan, S.H.L. Kok, D. Chan, M.Y.T. Tsoi, P.H.M. Leung, A.K.Y. Lam, A.S.C. Chan, K.H. Lam, J.C.O. Tang, Synthesis of 8-Hydroxyquinoline Derivatives as Novel Antitumor Agents, ACS Medicinal Chemistry Letters 4(2) (2013) 170-174.
[21] A.Y. Shaw, C.Y. Chang, M.Y. Hsu, P.J. Lu, C.N. Yang, H.L. Chen, C.W. Lo, C.W. Shiau, M.K. Chern, Synthesis and structure-activity relationship study of 8-hydroxyquinoline-derived Mannich bases as anticancer agents, European Journal of Medicinal Chemistry 45(7) (2010) 2860-2867.
[22] A.U. Rani, N. Sundaraganesan, M. Kurt, M. Cinar, M. Karabacak, FT-IR, FT-Raman, NMR spectra and DFT calculations on 4-chloro-*N*-methylaniline, Spectrochimica Acta Part A: Molecular and Biomolecular Spectroscopy 75(5) (2010) 1523-1529.
[23] A.D. Becke, Density-functional exchange-energy approximation with correct asymptotic behavior, Physical Review A 38(6) (1988) 3098-3100.
[24] A.D. Becke, A new mixing of Hartree–Fock and local density-functional theories, The Journal of Chemical Physics 98(2) (1993) 1372-1377.
[25] C. Lee, W. Yang, R.G. Parr, Development of the Colle-Salvetti correlation-energy formula into a functional of the electron density, Physical Review B 37(2) (1988) 785-789.
[26] S.V. G. M. Sheldrick, University of Gottingen, Germany.
[27] G. M. Sheldrick, Acta Crystallogr., Sect. A: Found. Crystallogr. 64 (2008) 112-122.
[28] G. M. Sheldrick, Acta Crystallogr. C, 71 (2015) 3-8.
[29] L.J.B. O.V. Dolomanov, R. J. Gildea, J. A. K. Howard and H. Puschmann, Journal of Applied Crystallography 42 (2009) 339-341.
[30] A. L. Spek, Acta Cryst D65 (2009) 148-155.
[31] M.J. Frisch, G.W. Trucks, H.B. Schlegel, G.E. Scuseria, M.A. Robb, J.R. Cheeseman, G. Scalmani, V. Barone, B. Mennucci, G.A. Petersson, H. Nakatsuji, M. Caricato, X. Li, H.P. Hratchian, A.F. Izmaylov, J. Bloino, G. Zheng, J.L. Sonnenberg, M. Hada, M. Ehara, K. Toyota,

R. Fukuda, J. Hasegawa, M. Ishida, T. Nakajima, Y. Honda, O. Kitao, H. Nakai, T. Vreven, J.A. Montgomery Jr., J.E. Peralta, F. Ogliaro, M.J. Bearpark, J. Heyd, E.N. Brothers, K.N. Kudin, V.N. Staroverov, R. Kobayashi, J. Normand, K. Raghavachari, A.P. Rendell, J.C. Burant, S.S. Iyengar, J. Tomasi, M. Cossi, N. Rega, N.J. Millam, M. Klene, J.E. Knox, J.B. Cross, V. Bakken, C. Adamo, J. Jaramillo, R. Gomperts, R.E. Stratmann, O. Yazyev, A.J. Austin, R. Cammi, C. Pomelli, J.W. Ochterski, R.L. Martin, K. Morokuma, V.G. Zakrzewski, G.A. Voth, P. Salvador, J.J. Dannenberg, S. Dapprich, A.D. Daniels, Ö. Farkas, J.B. Foresman, J.V. Ortiz, J. Cioslowski, D.J. Fox, Gaussian 09, Gaussian, Inc., Wallingford, CT, USA, 2009.
[32] I.R.D.J.I.E. NIST Computational Chemistry Comparison and Benchmark Database, NIST Standard Reference Database Number 101 Release, August 12, 2005, http://srdata.nist.gov/cccbdb.
[33] I.M. Alecu, J. Zheng, Y. Zhao, D.G. Truhlar, Computational Thermochemistry: Scale Factor Databases and Scale Factors for Vibrational Frequencies Obtained from Electronic Model Chemistries, Journal of Chemical Theory and Computation 6(9) (2010) 2872-2887.
[34] J. Tomasi, B. Mennucci, R. Cammi, Quantum Mechanical Continuum Solvation Models, Chemical Reviews 105(8) (2005) 2999-3094.
[35] I. Alkorta, J. Elguero, Structural Chemistry 9(3) (1998) 187-202.
[36] O. Meth-Cohn, B. Narine, A versatile new synthesis of quinolines, thienopyridines and related fused pyridines, Tetrahedron Letters 19(23) (1978) 2045-2048.
[37] B.F. Minaev, G.V. Baryshnikov, V.A. Minaeva, Electronic structure and spectral properties of the triarylamine-dithienosilole dyes for efficient organic solar cells, Dyes and Pigments 92(1) (2012) 531-536.
[38] MORPHY98, A program written by Popelier PLA with a contribution from Bone RGA. Manchester: UMIST (1998).
[39] N. Colthup, Introduction to infrared and Raman spectroscopy, Elsevier2012.
[40] S.E. Wiberley, N. Colthup, L. Daly, Introduction to infrared and Raman Spectroscopy, ed. NB Colthup and LH Daly, Academic Press, Inc., San Diego (1990).
[41] Y. Furukawa, M. Akimoto, I. Harada, Proceedings of the International Conference of Science and Technology of Synthetic Metals Vibrational key bands and electrical conductivity of polythiophene, Synthetic Metals 18(1) (1987) 151-156.
[42] B. Nolin, R.N. Jones, Canadian Journal of Chemistry 34(10) (1956) 1392-1404.
[43] G.C.B. M. Silverstein, C. Morill., Spectrometric Identification of Organic Compounds, (Wiley, New York,1981).
[44] S.I. Mizushima, T. Shimanouchi, K. Nakamura, M. Hayashi, S. Tsuchiya, C–Cl Stretching Frequencies in Relation to Rotational Isomerism, The Journal of Chemical Physics 26(4) (1957) 970-971.
[45] V. Arjunan, P.S. Balamourougane, C.V. Mythili, S. Mohan, Experimental spectroscopic (FTIR, FT-Raman, FT-NMR, UV–Visible) and DFT studies of 2-amino-5-chlorobenzoxazole, Journal of Molecular Structure 1003(1–3) (2011) 92-102.
[46] D.W. Moon, S.L. Bernasek, D.J. Dwyer, J.L. Gland, Observation of an unusually low carbon monoxide stretching frequency on iron(100), Journal of the American Chemical Society 107(14) (1985) 4363-4364.
[47] L. G, Proceedings of the XII International Conference on Raman Spectroscopy. Wurzburg, Germany. (1992).

[48] R.W. Mitchell, J.A. Merritt, Infrared and Raman spectra of methylene cyclopropane, Spectrochimica Acta Part A: Molecular Spectroscopy 27(9) (1971) 1609-1618.
[49] R. John Xavier, S. Ashok Raj, Ab initio, density functional computations, FT-IR, FT-Raman and molecular geometry of 4-morpholine carbonitrile, Spectrochimica Acta Part A: Molecular and Biomolecular Spectroscopy 101 (2013) 148-155.
[50] K. Malinakova, L. Novosadova, M. Lahtinen, E. Kolehmainen, J. Brus, R. Marek, 13C Chemical Shift Tensors in Hypoxanthine and 6-Mercaptopurine: Effects of Substitution, Tautomerism, and Intermolecular Interactions, The Journal of Physical Chemistry A 114(4) (2010) 1985-1995.
[51] I. Fleming, Frontier Orbitals and Organic Chemical Reactions, John Wiley and Sons, Berlin, (1976).
[52] K.S. J.S. Murray, Molecular Electrostatic Potentials, Concepts and Applications, Elsevier, Amsterdam, (1996).
[53] P.P. Singh, F.A. Pasha, H.K. Srivastava, DFT Based Atomic Softness and Its Application in Site Selectivity, QSAR & Combinatorial Science 22(8) (2003) 843-851.
[54] S.T. Schneebeli, M. Kamenetska, Z. Cheng, R. Skouta, R.A. Friesner, L. Venkataraman, R. Breslow, Single-Molecule Conductance through Multiple π–π-Stacked Benzene Rings Determined with Direct Electrode-to-Benzene Ring Connections, Journal of the American Chemical Society 133(7) (2011) 2136-2139.
[55] C. Ravikumar, I.H. Joe, V.S. Jayakumar, Charge transfer interactions and nonlinear optical properties of push–pull chromophore benzaldehyde phenylhydrazone: A vibrational approach, Chemical Physics Letters 460(4–6) (2008) 552-558.
[56] R.G. Pearson, Chemical hardness and density functional theory, Journal of Chemical Sciences 117(5) (2005) 369-377.
[57] T. Tsuneda, J.W. Song, S. Suzuki, K. Hirao, On Koopmans' theorem in density functional theory, The Journal of Chemical Physics 133(17) (2010) 174101.
[58] R.G. Parr, L.v. Szentpaly, S. Liu, Electrophilicity Index, Journal of the American Chemical Society 121(9) (1999) 1922-1924.
[59] S.V. Bondarchuk, B.F. Minaev, The singlet–triplet energy splitting of π-nucleophiles as a measure of their reaction rate with electrophilic partners, Chemical Physics Letters 607 (2014) 75-80.
[60] S.V. Bondarchuk, B.F. Minaev, State-Dependent Global and Local Electrophilicity of the Aryl Cations, The Journal of Physical Chemistry A 118(17) (2014) 3201-3210.
[61] J.P. R. Parthasarathi, V. Subramanian, B. Maiti, P.K. Chattraj,, Current Science 86 (2004) 535.
[62] D.R. Roy, U. Sarkar, P.K. Chattaraj, A. Mitra, J. Padmanabhan, R. Parthasarathi, V. Subramanian, S. Van Damme, P. Bultinck, Analyzing Toxicity Through Electrophilicity, Molecular Diversity 10(2) (2006) 119-131.
[63] Y. Ma, F. Wang, S. Kambam, X. Chen, A quinoline-based fluorescent chemosensor for distinguishing cadmium from zinc ions using cysteine as an auxiliary reagent, Sensors and Actuators B: Chemical 188 (2013) 1116-1122.
[64] S. Ou, Z. Lin, C. Duan, H. Zhang, Z. Bai, A sugar-quinoline fluorescent chemosensor for selective detection of Hg^{2+} ion in natural water, Chemical Communications (42) (2006) 4392-4394.